Journal of ELECTRONIC MATERIALS, Vol. 50, No. 6, 2021
https://doi.org/10.1007/s11664-021-08853-4

ORIGINAL RESEARCH ARTICLE

Fe-Cu Alloy-Based Flexible Electrodes from Ethaline Ionic Liquid

ABDULCABBAR YAVUZ ,[1,4] NECIP FAZIL YILMAZ,[2,3] and MURAT ARTAN[2]

1.—Department of Metallurgical and Materials Engineering, Gaziantep University, 27310 Sehitkamil, Gaziantep, Turkey. 2.—Department of Mechanical Engineering, Gaziantep University, 27310 Sehitkamil, Gaziantep, Turkey. 3.—Hasan Kalyoncu University, Board of Trustees, 27010 Gaziantep, Turkey. 4.—e-mail: ayavuz@gantep.edu.tr

The effective implementation of energy storage systems within flexible structures has recently become of particular interest. Here, the fabrication of inexpensive flexible electrodes via a number of straightforward methods formed the motivation for this research. Thin film-based Fe-Cu alloys were cathodically electrodeposited on a graphite substrate. As ionic liquids consist purely of ions (not solvent), they have recently been used in some electrochemical applications. In this study, therefore, Fe-Cu alloy coatings were prepared from an ethaline ionic liquid containing iron and copper salts. The electrochemical behaviour of Fe-Cu alloy films was determined by scanning between − 1.0 V and − 0.3 V in 1 M KOH at various scan rates ranging from 5 mV s^{-1} to 200 mV s^{-1}. These films were characterised in terms of their structural and morphological properties by means of Fourier transform infrared spectroscopy (FTIR), scanning electron microscopy (SEM) and x-ray diffraction (XRD). Formation of iron and copper alloy was differentiated depending on applied potential. The supercapacitive ability of Fe-Cu-coated film observed in 1 M KOH electrolyte demonstrated a specific capacitance of 304 F g^{-1} at a scan rate of 5 mV s^{-1}. The reaction between the alloy and the electrolyte was mainly controlled by a surface-controlled reaction. An asymmetric supercapacitor was constructed with an Fe-Cu-coated graphite negative electrode and a non-woven graphite positive electrode. Four asymmetric supercapacitors were connected in series and used to light up a blue light-emitting diode. This study shows that ethaline ionic liquid is a promising medium for the preparation of alloy-based electrodes in energy storage applications.

Key words: Supercapacitor, flexible, graphite, electrodeposition, ionic liquid

INTRODUCTION

Energy storage phenomena have in recent years received considerable attention due to the increasing energy requirements in today's world.[1,2] A rapidly growing population and improving technology necessitate high consumption of energy, which if left unaddressed could potentially lead to serious environmental problems and global warming.[3] For these reasons, decreasing the use of fossil fuels and generating new environmentally friendly and sustainable energy resources are of great importance. However, this also requires significant development of energy storage devices.[4] Economical, high-performance (specific power, energy and capacitance) energy storage devices with long-term stability have drawn considerable global attention.[5] Electrodes and electrolytes have been studied to reach these

(Received September 27, 2020; accepted February 27, 2021; published online March 26, 2021)

goals in batteries, fuel cells and supercapacitors.[6] Supercapacitors are considered to be amongst the more promising of energy storage devices because they typically have high power densities, long lives in terms of number of charging–discharging cycles, long-term usage with little requirement for maintenance and high conversion efficiency.[7,8]

Supercapacitors are referred to as ultracapacitors and can be classified into two main groups: electrochemical double-layer capacitors (EDLCs),[9] and pseudocapacitors.[10] Recently, supercapacitors have been used in applications such as buses, tramways, trolleybuses, industrial equipment, electronic devices, solar arrays, and wind turbines.[11] In particular, the usage of supercapacitors in the automotive industry could drastically increase the efficiency of hybrid electric vehicles.[12]

It has been suggested that supercapacitors have a number of unique advantages including high specific power (shorter charge and discharge times), cycling stability, and low maintenance costs compared to other energy storage devices. However, they also have a number disadvantages, but in particular have low energy densities compared to batteries and fuel cells[13] Various attempts have been made to increase the energy densities of supercapacitors.[14,15] The energy density (E) of a capacitor can be found by $E = 1/2\ CV^2$, where C is the capacitance and V is the cell potential. According to this equation, increasing the potential or capacitance results in a higher energy density.[16] To increase the specific capacitance of a supercapacitor, the surface area of the electrode materials must be as high as possible to improve the flux of ions to and from the electrode and to reserve a large amount of electroactive species in faradaic redox reactions or EDLC systems.[17] Carbon-based materials are commonly used in EDLC. However, metal oxide/hydroxides and conductive polymers can be applied as pseudocapacitor electrodes.[18,19,20]

The electrochemical specification of the anode and cathode material, potential range, and electrolyte are the main factors one needs to consider in order to obtain a high performance supercapacitor.[21] Metal oxides are generally the primary candidates for the electrode material since the oxidation numbers of the metals can vary depending on redox potential. Metal oxides also have high mechanical and chemical stability in the electrolytes, and can also have high specific and areal capacitances with specific powers because of their multiple oxidation states. Various metal oxides have been examined for suitability in supercapacitor applications such as the oxide and hydroxide forms of metals, including those of iron,[22] nickel,[23,24] manganese,[25] tungsten,[26] tin,[27] ruthenium,[28] copper,[29] and cobalt.[30] The key requirements in building a supercapacitor electrode include low cost and good performance of the electrodes. Therefore, copper and iron, which are easily extracted, have been studied as electrode materials herein.

Supercapacitors can have several important advantages in terms of high power delivery capability and high stability. Therefore, they have gained significant attention from researchers in terms of studying the energy demands of a wide range of devices such as mobile phones, notebooks, wearable devices, paper and textile based devices, medical devices, and electric vehicles.[31] For these applications, flexible energy storage electrodes are required for wearable paper- and textile-based devices.[32,33,34] Flexible energy storage systems have a number of applications in medical devices, military equipment, safety and construction equipment, and wearable electronic devices to provide power.[35] The development of a suitable flexible, high performance supercapacitor is a critical challenge. On the other hand, the need for a flexible and conductive substrate for use as a current collector is also a key issue for flexible devices. The ideal substrates for electrodes used in wearable electronics (e-textiles) would be paper- and textile-based materials because of their flexibility, porous structure, and low cost. However, these substrates have an insulating nature and must be coated with a conductive material, such as silver nanowires or carbon nanotubes, in order to enable electricity to be conducted.

Recently, a number of studies have attempted to produce flexible supercapacitor systems because of the rapid development of portable and wearable devices. One such attempt was to fabricate graphene-based flexible supercapacitor systems.[36,37,38] Graphene is one of the more essential materials required to fabricate flexible electrodes because it has an extremely high mechanical strength, high electrical conductivity, and an exceptionally high surface area. It provides a high sustainability under mechanical bending and twisting. However, the methods for development of graphene-based electrodes are demanding. Therefore, a straightforward and inexpensive method that would allow the construction of a flexible electrode is required.

The objective of this research is to produce an electroactive and stable Fe-Cu mixed film on graphite electrode surfaces by applying different voltages across a plating bath. The iron- and copper-based films electrochemically deposited on the graphite electrodes were examined in a potassium hydroxide electrolyte to demonstrate their supercapacitor performance. In order to analyse the effects of the applied potentials, the redox reactions of the Fe-Cu-coated films in alkaline electrolytes were examined and the compositions, structures, and surface morphologies of the electrodes studied by varying the applied potentials.

EXPERIMENTS

Ethaline (a deep eutectic solvent ionic liquid) was used as a deposition medium in this study. Ethaline was prepared by mixing and heating one part choline chloride with two parts ethaline glycol until a homogenous liquid solution was obtained. 0.1 M iron (II) sulphate (99% $FeSO_4$) and 0.1 M copper (II) chloride (99% $CuCl_2$) were prepared in ethaline. The electrodeposition of copper and iron was carried out on graphite electrodes. A platinum wire reference electrode and platinum counter electrode were used during the deposition of metals in the ethaline electrolyte. The thickness of the graphite sheets was 1 mm. The Fe-Cu deposition solution was heated to 65°C and Fe-Cu alloy was electrodeposited potentiostatically by applying different voltages (from − 2.0 V to − 1.2 V) for 5 minutes. The Fe-Cu-coated electrode was then washed to remove any possible impurities from the deposition bath and dried using a tissue. Fe-Cu alloy films were cycled between − 1.0 V and − 0.3 V in 1 M KOH at various scan rates ranging from 5 mV s^{-1} to 200 mV s^{-1} in order to elucidate the associated electrochemical performance and behaviour. All cycling experiments were carried out at room temperature (25 ± 2°C) in this study. All electrochemical experiments were implemented using a conventional three-electrode potentiostat (AMETEK VersaSTAT 3, USA). The working electrode was graphite coated with an Fe-Cu film, whilst the reference electrode was changed to Ag-AgCl (in saturated KCl) in the alkaline bath. The counter electrode was platinum for all aqueous and ionic liquid electrochemical measurements. Galvanostatic charge–discharge of the coated electrode was performed in alkaline solution by applying a constant current. The positive and negative electrodes were formed from a nonwoven graphite fabric and Cu-Fe coated graphite, respectively. The Fourier transform infrared (FTIR) spectra of the uncoated and Fe-Cu-coated electrodes were obtained using a Shimadzu IRTracer-100. The surface morphology of deposited alloy coatings and bare graphite electrode were examined using FEG-SEM (Zeiss Sigma 300). The structures of the uncoated and alloy-coated modified electrodes were analysed using a PANalytical Empyrean XRD spectrometer with 1.54 Å Cu Kα source.

RESULTS AND DISCUSSION

The cyclic voltammetry of the graphite electrode was carried out in an ethaline electrolyte in order to investigate the optimal electrochemical deposition conditions for copper and iron. The graphite electrode film was first scanned in pure ethaline at room temperature and subsequently at 65°C in order to visualize the potential window, as illustrated by the black line in Fig. 1a. Graphite was cycled in ethaline containing 0.1 M $FeSO_4$, with its cyclic voltammogram response illustrated as the red line in Fig. 1a. The cycling of graphite in ethaline with Fe^{2+} ions was initiated with an open circuit potential to − 2.0 V and then scanned to 1.0 V at a scan rate of 20 mV s^{-1} at room temperature. The reduction peak that appeared at around − 0.8 V (given as Fe-1 in the red line in Fig. 1a) is related to the reduction of Fe^{2+} because a reduction peak was not observed when graphite was cycled in a pure ethaline electrolyte. Reduction of iron was significant at the potential which was more negative than − 1.5 V. The current required for graphite cycling in ethaline having Fe^{2+} ions (shown as Fe-2 in Fig. 1a) was greater than that required in pure ethaline (given as E-2 in Fig. 1a) because the electrodeposited metals caused the evolution of hydrogen.[39] The reduction observed

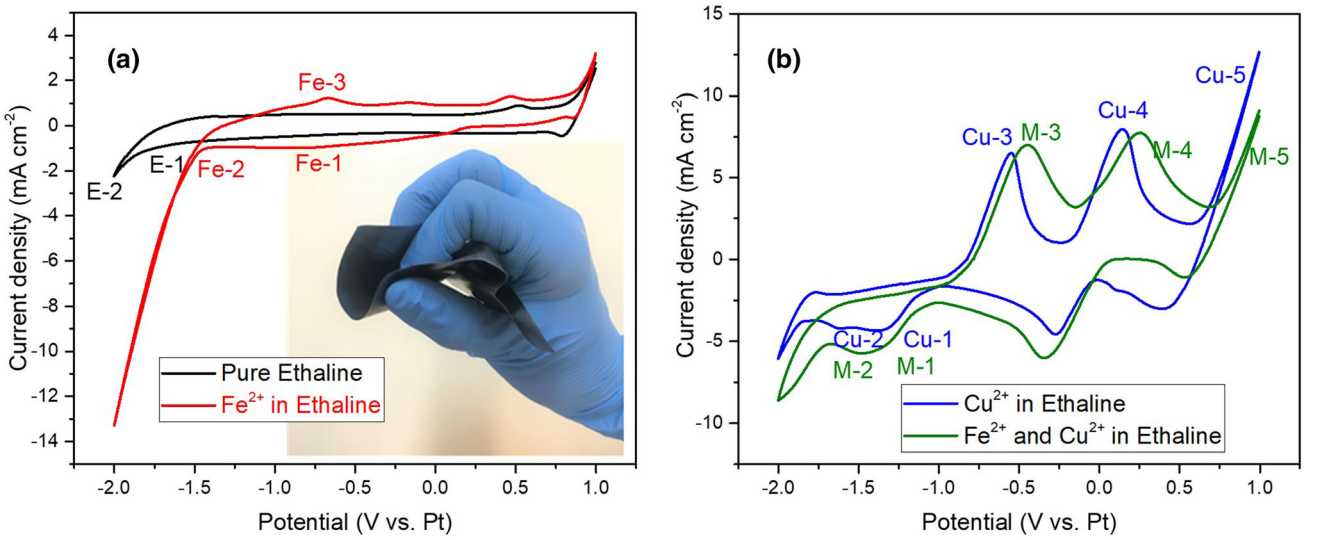

Fig. 1. Cyclic voltammograms of graphite in (a) pure ethaline (black line), 0.1 M Fe^{2+} in ethaline (red line) and (b) 0.1 M Cu^{2+} in ethaline (blue line), and 0.1 M Fe^{2+} and 0.1 M Cu^{2+} in ethaline (green line) at room temperature at a scan rate of 20 mV s^{-1}. Inset: illustration of the flexible graphite electrode used in these cyclic voltammogram experiments (Color figure online).

around − 1.5 V was related to hydrogen evolution because the magnitude of the iron oxidation (indicated as Fe-3 in the red line in Fig. 1a) corresponded to the reduction peak in Fe-1 (of Fig. 1a). A graphite working electrode was used in this experiment as such electrodes are not electrochemically active (black line in Fig. 1a). Graphite was cycled in a 0.1 M $CuCl_2$ contained ethaline bath, with the resultant cyclic voltammogram illustrated as the blue line in Fig. 1b. The cyclic voltammogram of graphite in ethaline with Cu^{2+} ions shows two distinct reduction processes that could be observed around − 0.25 V, the reduction of Cu^{2+} to Cu^{+}, and at − 1.2 V, the reduction of Cu^{+} to metallic Cu. The cyclic voltammogram of ethaline with Fe^{2+} (red line in Fig. 1a) and Cu^{2+} (blue line in Fig. 1a) separately shows that the application of a constant potential at less than − 1.2 V would result in the growth of Fe-Cu alloy. The oxidation peaks observed at around − 0.6 V and 0.2 V can be attributed to the oxidation of Cu to Cu^{+} and Cu^{+} to Cu^{2+}, respectively; this will not be considered further herein, but a detailed explanation of copper deposition/dissolution can be found in the literature.[40,41,42] The graphite electrode film was also cycled in ethaline electrolyte solution with 0.1 M Fe^{2+}- and 0.1 M Cu^{2+}-based salts. The cyclic voltammograms of this mixture were cycled between − 2.0 V and 1.0 V at a scan rate of 20 mV s^{-1} at room temperature, as shown by the green line in Fig. 1. The cyclic voltammogram of graphite in ethaline electrolyte containing both iron and copper ions was similar to that observed for ethaline containing copper ions.

Surface characterization of Fe-Cu-coated films was carried out via XRD, FTIR, Raman, and SEM analyses. Fe-Cu coatings were electrodeposited from ethaline containing 100 mM Cu^{2+} and 100 mM Fe^{2+} by application of − 1.2 V, − 1.4 V, − 1.6 V, − 1.8 and − 2.0 V for 300 seconds at 65°C. The surface morphologies of the films so produced were investigated via SEM. Figure 2 shows the SEM images of the Fe-Cu-coated films at 25000× magnification. Figure 2a to e shows the films electrodeposited at different deposition potentials (− 1.2 V, − 1.4 V, − 1.6 V, − 1.8 V and − 2.0 V). Rough irregular agglomerated particles were observed for all the coatings shown in Fig. 2. EDX mapping of the coating electrodeposited from ethaline containing copper and iron ions by application of − 2.0 V is presented in Fig. 2f. According to the EDX analysis for the latter, the composition consisted of 53% Cu and 47% Fe. EDX analyses of Fe-Cu-coated films electrodeposited from ethaline ionic liquid due to the application of different voltages are illustrated in Fig. 3. Fe-Cu alloys were electrodeposited on graphite surfaces in order to observe only the electrodeposited elements.[43] Electrodeposition of Fe-Cu alloys was performed on graphite surfaces, as shown in the inset in Fig. 1a, with the percentage of iron and copper in the alloys on the graphite surfaces shown in Fig. 3. These results depict the fact that applying a more negative voltage to a graphite electrode in ethaline will generally give a higher ratio of copper in the resultant Fe-Cu alloy system.

In order to analyse the crystal structure of the coated films, XRD analysis was carried out for both the uncoated graphite and the Fe-Cu-coated films obtained at different deposition voltages on graphite substrates. The XRD analyses for the uncoated and Fe-Cu-coated graphite electrodes are presented in Fig. 4. The XRD peaks for the alloys are not clearly

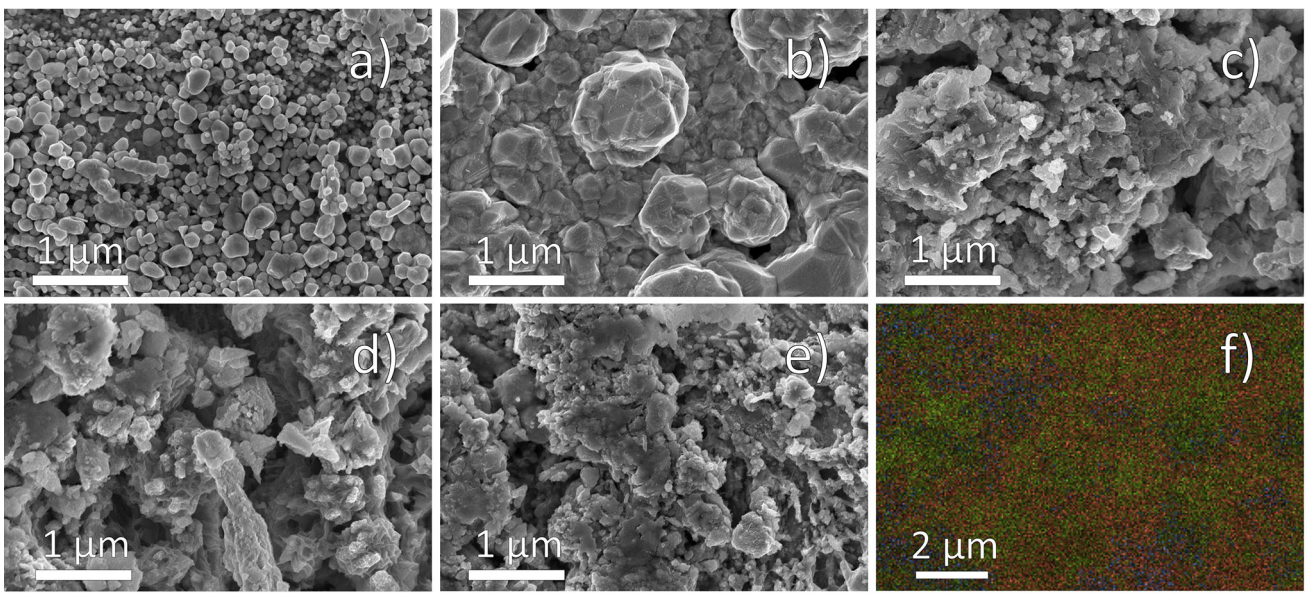

Fig. 2. SEM images of coatings electrodeposited from ethaline containing 100 mM Fe^{2+} and 100 mM Cu^{2+} by applying (a) − 1.2 V; (b) − 1.4 V; (c) − 1.6 V; (d) − 1.8 V and; (e) − 2.0 V. The potential was applied for 5 minutes to grow each coating. (f) EDX mapping of the Fe-Cu film electrodeposited at − 2.0 V. Green and red dots represent elemental copper and iron (Color figure online).

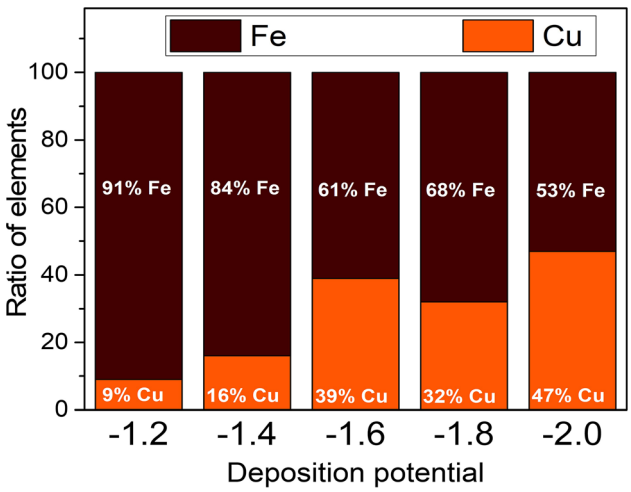

Fig. 3. EDX analyses of the Fe-Cu alloy films presented in Figure 2.

comparable in Fig. 4a. Therefore, XRD peaks of alloys coated graphite are compared with those of uncoated graphite at high magnification in Fig. 4b and c. A diffraction peak that appeared at 51° corresponds to the face-centred cubic (fcc) structure of Cu (200), which was indexed according to the standard JCPDS No. 04-0836.[44,45] The coated graphites also showed peaks at 44° (black line), which was characteristic of alpha-iron.[46] Peaks that could be attributed to iron potentially indicated the electrodeposition of iron with copper. The possible codeposition of Cu and Fe described above was further demonstrated by EDX and XRD analyses, which also indicate that copper was electrodeposited with iron.

FTIR spectra of the samples were recorded in order to elucidate the electrode composition further. Figure 5 shows the FTIR spectra for the bare

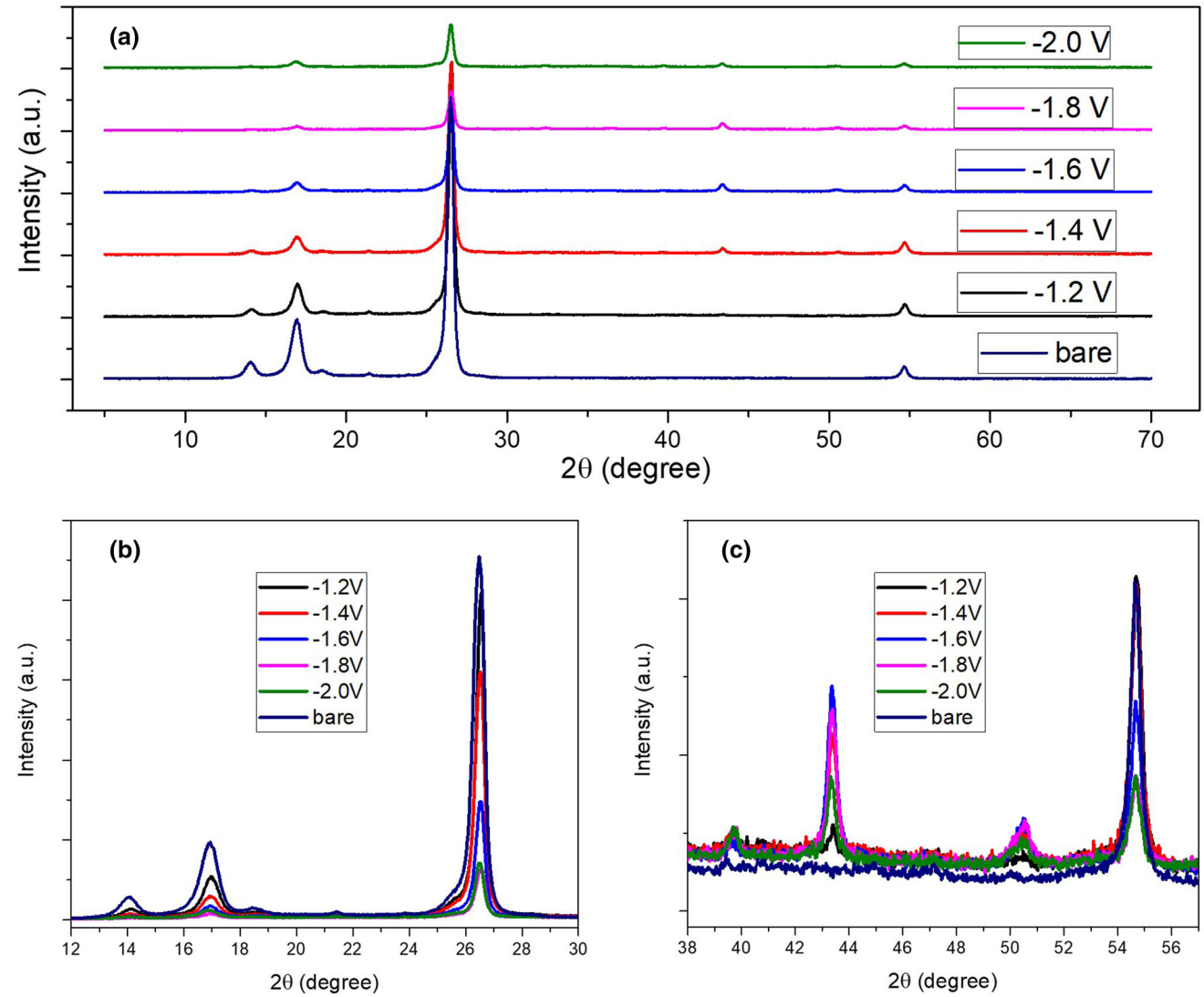

Fig. 4. (a) XRD analysis of the bare graphite (dark blue line) and Fe-Cu-coated films on graphite obtained by applying different deposition potentials. XRD peaks for the electrodes presented in panel a are shown at higher magnification in panel b and panel c. Deposition potentials are indicated in the figures (Color figure online).

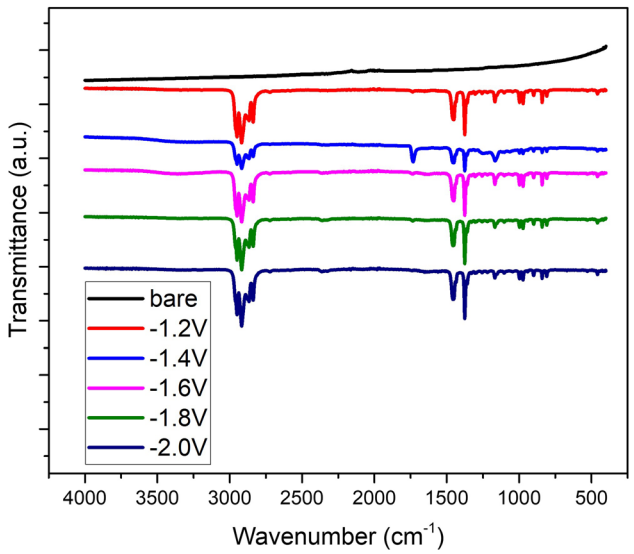

Fig. 5. FTIR spectra of bare graphite and Fe-Cu electrodeposited on a graphite surface by applying different deposition potentials. Deposition potentials are indicated in the figure.

graphite and Fe-Cu-coated films electrodeposited from ionic liquid using different voltages. The peaks observed between 400 cm^{-1} and 1500 cm^{-1} on the graphite substrate for the electrodes obtained at different potentials were recognized as Cu-O and Fe-O vibrations.[47] These peaks confirmed the formation of copper oxide[48] and iron oxide,[49] which probably formed as a thin oxidation coating at the surface of the alloys at room conditions. The peaks belonging to the oxide forms of the metals were not particularly intense, which could have been present merely as a thin film on the alloy surface. The peaks at around 3000 cm^{-1} likely indicate the presence of water due to adsorption of moisture at room conditions.[50]

SEM, EDX, XRD and FTIR characterizations of the Fe-Cu coated films are presented above. The films electrodeposited from ionic liquid media were immersed in 1 M KOH electrolyte for electrochemical characterization. Figure 6a illustrates the cyclic voltammetric curves of Fe-Cu alloy on graphite substrate film electrodeposited from ionic liquid by the application of − 1.8 V and cycled in KOH electrolyte between − 1.0 V and − 0.3 V at scan rates ranging from 5 mV s^{-1} to 200 mV s^{-1}, as illustrated in Fig. 6a. This figure is presented here representatively, as the cyclic voltammograms of all Fe-Cu films electrodeposited by applying different potentials were all very similar. The cyclic voltammetry of the film displayed in Fig. 6a shows that the film cycled in alkaline media provided reversibility, with the degree of reversibility presented below. Figure 6b displays the specific capacitances of the Fe-Cu-coated film at various scan rates using the cyclic voltammogram curve graphs presented in Fig. 6a. The specific capacitance, C_p (F g^{-1}), of the Fe-Cu coated modified electrode was calculated via Eq. 1:[51,52]

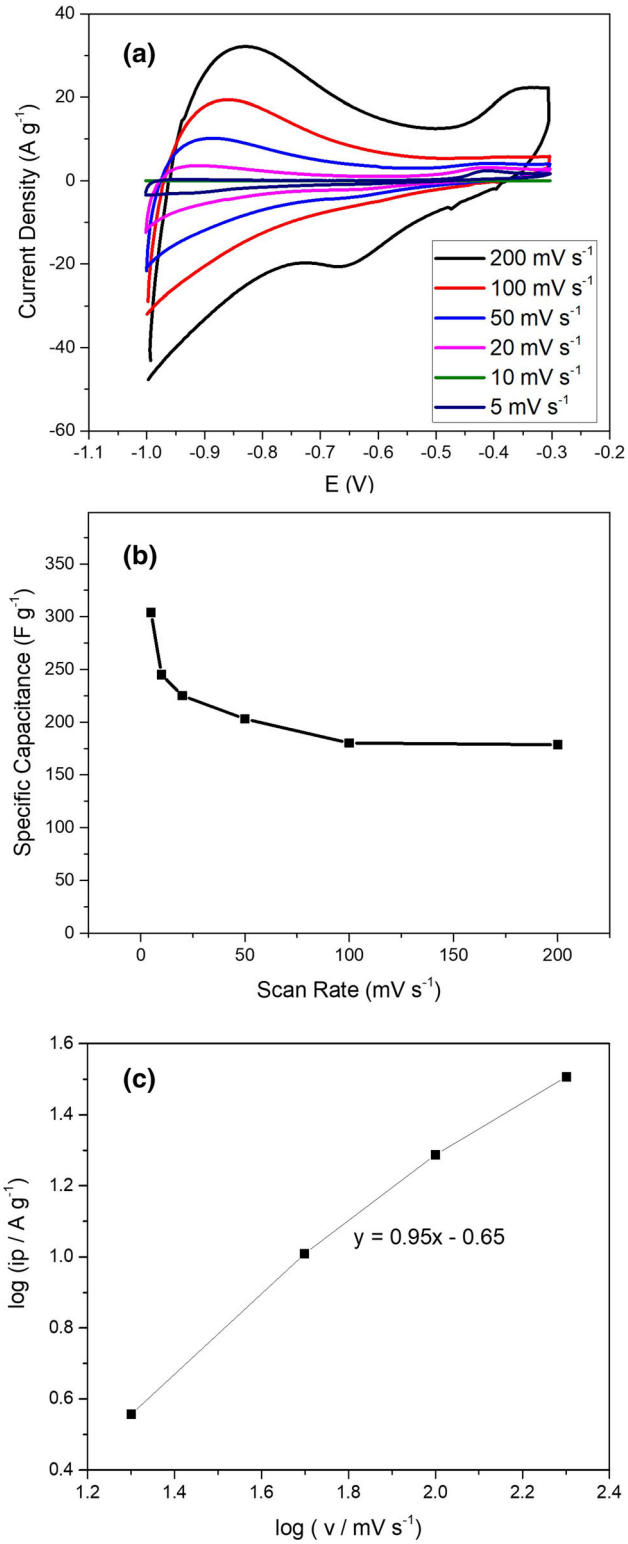

Fig. 6. (a) Cyclic voltammogram of Fe-Cu alloy films on graphite cycled in 1 M KOH electrolyte at scan rates of 5, 10, 20, 50, 100 and 200 mV s^{-1}. (b) Specific capacitance of Fe-Cu electrodes as a function of scan rate. Specific capacitance was calculated using Eq. 1 with data from in (a). (c) Logarithm of maximum points of current peaks as a function of logarithmic scan rates. Data were taken from (a).

$$C_p = \frac{1}{mv(V_2 - V_1)} \int_{V_1}^{V_2} I(V)\mathrm{d}V \quad (1)$$

where m is the electroactive mass of the Fe-Cu film, v is the scan speed (V s^{-1}), $V_2 - V_1$ is the potential range of the cyclic voltammogram, and I is the current (A). Specific capacitance reached a maximum of 304 F g^{-1} at a scan rate of 5 mV s^{-1}. The film was found to have a capacitance of 180 F g^{-1} and 198 F g^{-1} at scan rates of 100 and 200 mV s^{-1}, respectively.

A plot of the logarithm of the cathodic peak current density of the electrode against the logarithm of scan rate given in Fig. 6a is illustrated in Fig. 6c. This graph is necessary to understand the rate limiting reaction. When an electrochemical reaction occurs, three main reaction mechanisms are possible between the surface of the electrode films and the electrolyte, namely the kinetically controlled, surface-controlled, and diffusion-controlled. Using the Cottrell equation (Eq. 2), the diffusion-controlled can be determined to be the predominant mechanism in the electrochemical reactions

$$i = \frac{nFAc_0\sqrt{D}}{\sqrt{\pi t}}, \quad (2)$$

where i is the current (in amperes), D is the diffusion coefficient (cm^2 s^{-1}), F is the Faraday constant (96485 C mol^{-1}), n is number of electrons passing between the electrode and electrolyte, c_0 is the initial molarity of the ions diffusing between electrode and electrolyte (mol.cm^{-3}), A is the electrode area (in cm^2), and t is the time (s). According to Eq. 2, current response is dependent upon time, and if the current (i) is proportional to $\sqrt{1/t}$, it can be understood that the reaction is diffusion-controlled. In the instance of rapid diffusion of the species in question between the electrode and the electrolyte, the reaction would be kinetically controlled and thus unsuitable for energy storage devices because electron transfer in such situations is slow. If the slope of the logarithm peak current against the logarithm scan rate is less than 0.5, the reaction is considered to be kinetically controlled; if, however, the gradient is equal to 0.5, it is considered to be completely diffusion-controlled, as can be determined from Eq. 2. If the gradient of the logarithm peak current against the logarithm of the scan rate is equal to 1, then the reaction is completely surface-controlled, with gradients between 0.5 and 1 considered to be a mixture of both diffusion- and surface-controlled reaction mechanisms. According to Fig. 6c, the slope of the logarithm scan rate versus the logarithm of the peak current is equal to 0.95, and, further, the current peak value was not proportional to $t^{-1/2}$. Therefore, the reaction does not follow a kinetically controlled mechanism and can be used in energy storage devices. Because the gradient is close to 1, its reaction is mainly controlled by a surface adsorption-like reaction, which is suitable for energy storage devices. The supercapacitive performances of copper- and iron-based electrodes are compared with the results of this study in Table I.

Figure 7a displays the galvanostatic charge–discharge curves for the Fe-Cu alloy electrodeposited on graphite from ethaline by the application of a constant potential of − 1.8 V. The charge/discharge curve for the Fe-Cu alloy graphite electrode has a triangle-like profile, which is indicative of the capacitive-like behaviour of the electrode. Figure 7b illustrates the specific capacitance of the electrode calculated from the data given in Fig. 7a. The specific capacitances of the two cells (Fig. 7b) was lower than that of three cells (Fig. 6b) because the calculation for the latter focuses on only one electrode (working electrode), while that for the former focuses on the entire electrode, which is more realistic. The self-discharge rate of a supercapacitor is an important factor in practical applications.[53,54] Figure 7c presents the self-discharge curve for the Fe-Cu alloy graphite electrode. The electrode was first charged to either 1.0 V or 1.4 V for 10 minutes and then left to allow it to undergo self-discharge. It was observed that the potential of the electrodes charged to 1.0 V and 1.4 V decreased to around 0.2 V

Table I. Supercapacitor performance of copper- and iron-based electrodes presented in the literature

Electrode	Method of synthesis	Capacitance	References
Copper oxide	Cathodic deposition	36 F g^{-1}	55
Copper oxide	Sonochemical assisted precipitation	125 F g^{-1}	56
Fe_2O_3 nanoflower	Ethylene glycol mediated self-assembly process	127 F g^{-1}	57
Fe_2O_3 nanotube	Anodization	138 F g^{-1}	58
Copper oxide	Chemical bath deposition	43 F g^{-1}	50
CuO	Mechanochemical method	114 F g^{-1}	59
CuO	Potentiodynamic deposition	179 F g^{-1}	60
Fe_2O_3	Sol–gel	300 F g^{-1}	61
Fe_2O_3	SILAR method	178 F g^{-1}	49
Iron and copper alloy	Electrodeposition	304 F g^{-1}	This work

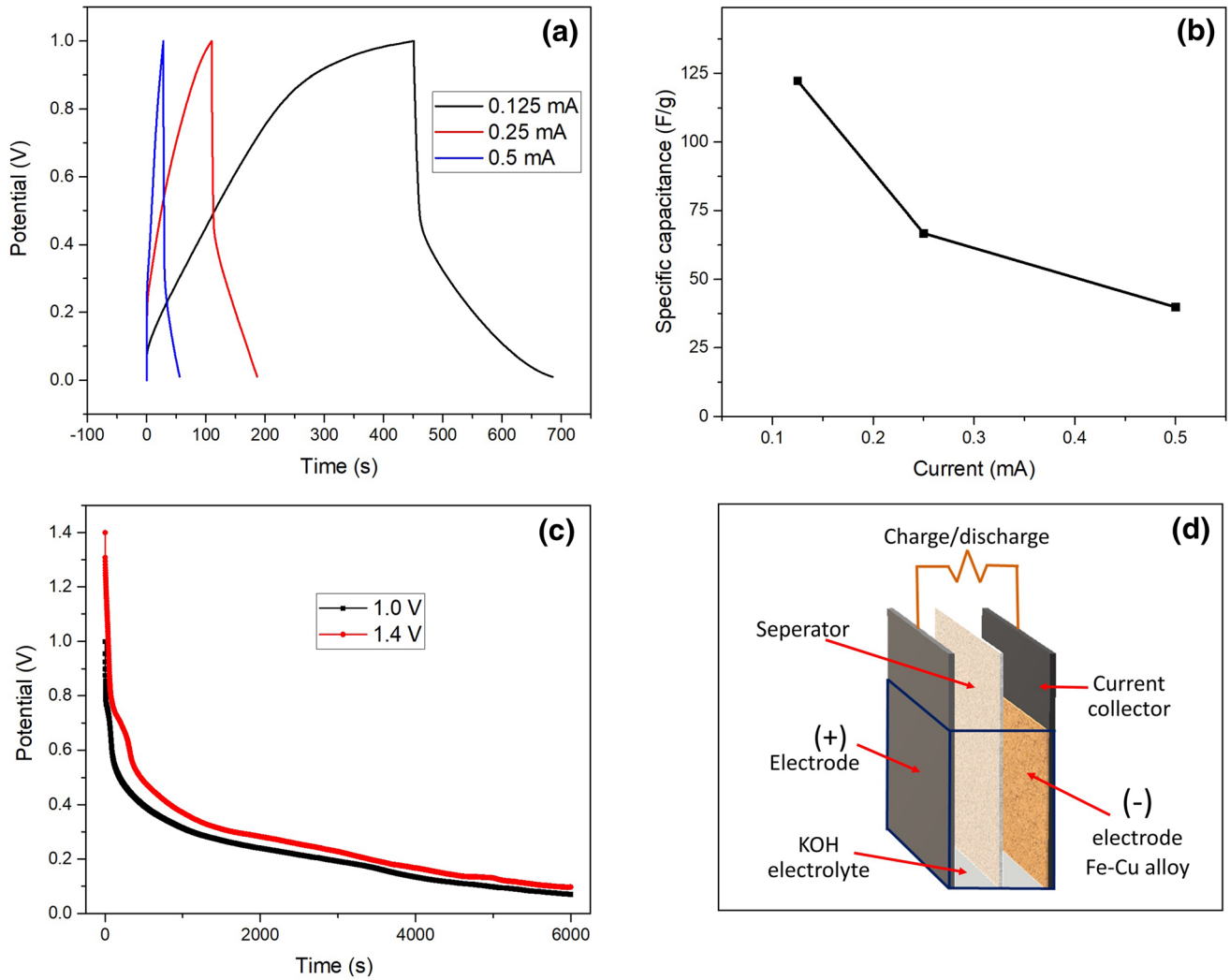

Fig. 7. (a) Charge-discharge curve for the Fe-Cu alloy on graphite electrode electrodeposited at − 1.8V. (b) Specific capacitance of a Fe-Cu electrode as a function of scan rate. Specific capacitance was calculated from the data given in panel a. (c) Self-discharge curve for the Fe-Cu alloyed graphite electrode. (d) Schematic representation of the device assembly used to find the results shown in panel a and panel c.

after an hour self-discharge. Generally, metal oxide-based electrodes that can be used for supercapacitor electrodes suffer from self-discharge problems. A schematic representation of the assembly of the device used for the galvanostatic charge–discharge and self-discharge experiments is presented in Fig. 7d.

Figure 8a illustrates the cyclic voltammogram of the flexible alloy-coated graphite to test the electrochemical response of the film at bending angles of 0°, 90° and 180°. The cyclic voltammetric responses of the flexible electrode at different bending angles shown in Fig. 8a were identical, indicating that the electrochemical behaviour of the modified electrode was not significantly affected when mechanical bending was induced. Figure 8c, d and e illustrate the preparation of a flexible electrode with Fe-Cu-coated graphite in order to illuminate a blue LED lamp. The graphite surface was coated with Fe-Cu alloy via electrodeposition and used as a negative electrode. Non-woven graphite fabric was used as a positive electrode. 1 M KOH solution was poured over both the Fe-Cu-coated graphite electrode and the dielectric separator (nonwoven polypropylene). A dielectric separator was inserted between two flexible graphite electrodes and then taped to avoid the liquid escaping. A 2.2 V blue LED lamp was illuminated successfully with the flexible electrode so constructed.

CONCLUSIONS

Fe-Cu alloyed films cathodically electrodeposited from ethaline solution on a flexible graphite electrode have been developed for supercapacitor applications. $FeSO_4$ and $CuCl_2$ were dissolved in ethaline to prepare it as a deposition electrolyte. Flexible graphite electrodes were potentiostatically electrodeposited by applying different voltages in the range of − 2.0 V and − 1.2 V. Coated films were

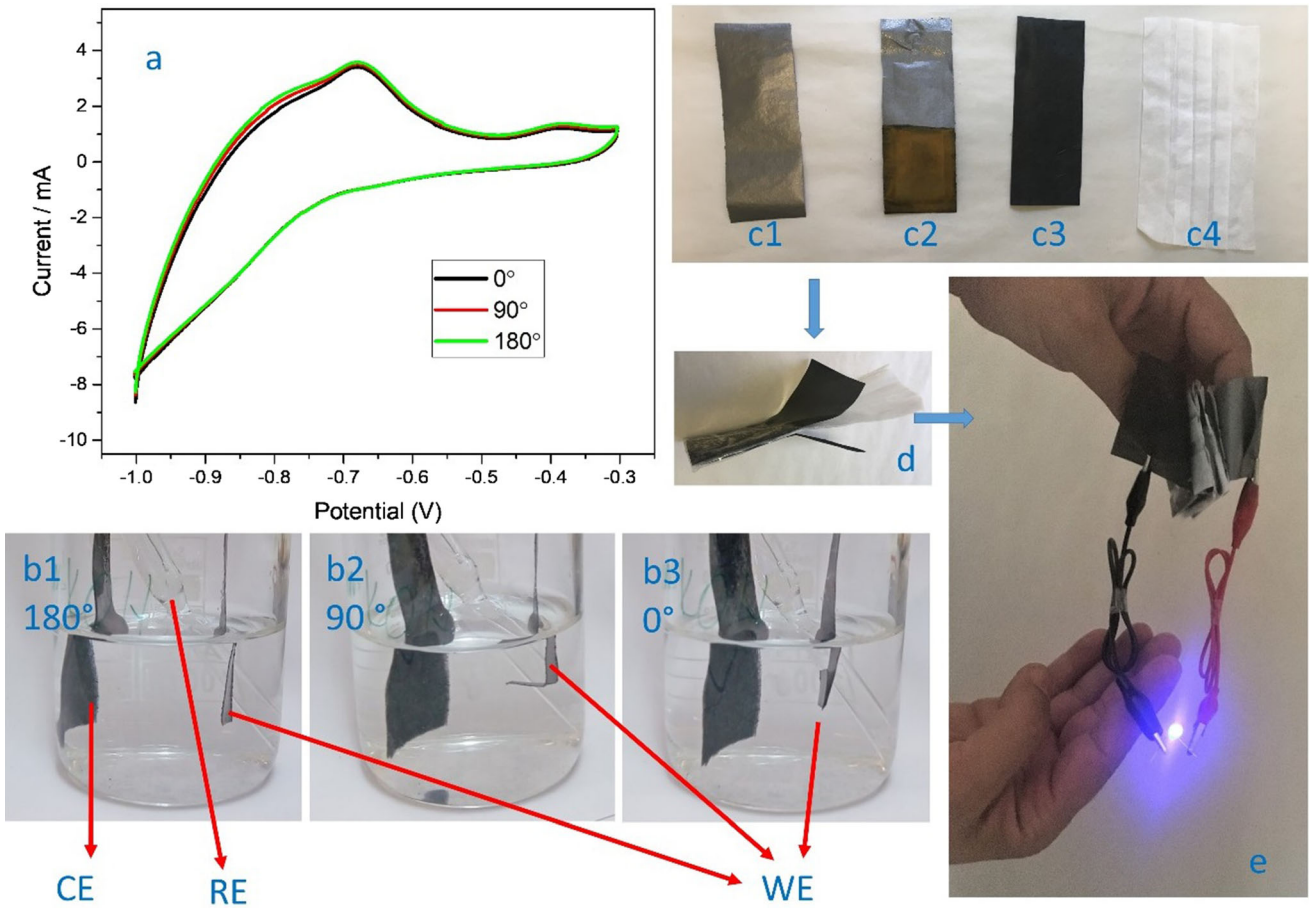

Fig. 8. (a) Cyclic voltammograms of Fe-Cu-coated graphite electrode bent at angles of 180° (panel b1), 90° (panel b2) and 0° (panel b3) cycling in KOH. (WE: working electrode; CE: counter electrode; RE: reference electrode) Blue LED lamp illumination using a flexible supercapacitor. Photo of (c1) bare graphite; (c2) flexible graphite electrode coated with Fe and Cu by electrodeposition and used as a negative electrode; (c3) flexible graphite-based nonwoven cloth used as a positive electrode; (c4) dielectric nonwoven polypropylene separator. (d) Photo of flexible supercapacitor constructed. (e) Photo of the blue LED lamp with the constructed flexible supercapacitor after connection to each other.

transferred into a 1 M KOH electrolyte and scanned over a negative potential range between − 1.0 V and − 0.3 V by applying various scan rates ranging from 5 mV s^{-1} to 200 mV s^{-1} to investigate the electrochemical performance and behaviour of alloy-based electrodes. Non-electrochemical *ex situ* (FTIR, XRD and SEM) analyses were carried out in order to gain the compositional, structural, and morphological characterizations of the films. FTIR, EDX, and XRD results confirmed the formation of Fe and Cu alloys from ionic liquid solutions. Fe-Cu films exhibited a specific capacitance of 304 F g^{-1} at a scan rate of 5 mV s^{-1}. The reaction mechanisms between the Fe-Cu coated electrode and KOH electrolyte suggested a surface-controlled mechanism, which is desirable for energy storage devices.

ACKNOWLEDGMENTS

M. A. would like to thank YÖK for his PhD scholarship. The authors also thank the Scientific Research Project Unit at Gaziantep University (MF.ALT.19.18).

CONFLICT OF INTEREST

The authors declare that they have no conflict of interest.

REFERENCES

1. T. Chen, and L. Dai, *Mater. Today* 16, 272 (2013).
2. R. Amirante, E. Cassone, E. Distaso, and P. Tamburrano, *Energy Convers. Manag.* 132, 372 (2017).
3. K. Wang, H. Wu, Y. Meng, and Z. Wei, *Small* 10, 14 (2014).
4. H. Ibrahim, A. Ilinca, and J. Perron, *Renew. Sustain. Energy Rev.* 12, 1221 (2008).
5. K. Zhang, M. Liu, T. Zhang, X. Min, Z. Wang, L. Chai, and Y. Shi, *J. Mater. Chem. A* 7, 26838 (2019).
6. S. Koohi-Fayegh, and M.A. Rosen, *J. Energy Storage* 27, 101047 (2020).
7. J. Wang, Y. Xu, J. Zhu, and P. Ren, *J. Power Sources* 208, 138 (2012).
8. P. Simon and Y. Gogotsi, in *Nanoscience and Technology: a Collection of Reviews from Nature Journals*, ed. by P. Rodgers (World Scientific, London, 2010), pp. 320–329.
9. V.V.N. Obreja, *Phys. E Low-Dimens. Syst. Nanostruct.* 40, 2596 (2008).
10. S. EzhilArasi, R. Ranjithkumar, P. Devendran, M. Krishnakumar, and A. Arivarasan, *J. Mater. Sci. Mater. Electron.* 31, 7012 (2020).
11. A. Muzaffar, M.B. Ahamed, K. Deshmukh, and J. Thirumalai, *Renew. Sustain. Energy Rev.* 101, 123 (2019).

12. Y.H. Kim, S.W. Kim, and S.-H. Lee, *J. Power Sources* 114, 366 (2003).
13. G. Wang, L. Zhang, and J. Zhang, *Chem. Soc. Rev.* 41, 797 (2012).
14. A. Burke, *J. Power Sources* 91, 37 (2000).
15. J.R. Miller, and P. Simon, *Sci. Mag.* 321, 651 (2008).
16. R. Kötz, and M. Carlen, *Electrochim. Acta* 45, 2483 (2000).
17. C.D. Lokhande, D.P. Dubal, and O.-S. Joo, *Curr. Appl. Phys.* 11, 255 (2011).
18. S.R.C. Vivekchand, C.S. Rout, K.S. Subrahmanyam, A. Govindaraj, and C.N.R. Rao, *J. Chem. Sci.* 120, 9 (2008).
19. R. Ramya, R. Sivasubramanian, and M.V. Sangaranarayanan, *Electrochim. Acta* 101, 109 (2013).
20. X. Lang, A. Hirata, T. Fujita, and M. Chen, *Nat. Nanotechnol.* 6, 232 (2011).
21. J. Yan, Q. Wang, T. Wei, and Z. Fan, *Adv. Energy Mater.* 4, 1300816 (2014).
22. K.A. Owusu, L. Qu, J. Li, Z. Wang, K. Zhao, C. Yang, K.M. Hercule, C. Lin, C. Shi, and Q. Wei, *Nat. Commun.* 8, 1 (2017).
23. H. Jiang, T. Zhao, C. Li, and J. Ma, *J. Mater. Chem.* 21, 3818 (2011).
24. A. Yavuz, K. Kaplan, M. Bedir, and J. Dig, *Nanomater. Biostruct.* 14, 1061 (2019).
25. J. Liang, B. Tian, S. Li, C. Jiang, and W. Wu, *Adv. Energy Mater.* 10, 2000022 (2020).
26. J. Chen, H. Wang, J. Deng, C. Xu, and Y. Wang, *J. Mater. Chem. A* 6, 8986 (2018).
27. A. Yavuz, K. Kaplan, and M. Bedir, *J. Electroanal. Chem.* 877, 114635 (2020).
28. K. Krishnamoorthy, P. Pazhamalai, and S.J. Kim, *Electrochim. Acta* 227, 85 (2017).
29. A. Esfandiar, M. Qorbani, I. Shown, and B.O. Dogahe, *J. Mater. Chem. A* 8, 1920 (2020).
30. P. Sivakumar, M. Jana, M. Kota, M. Gyu, A. Gedanken, and H. Seok, *J. Power Sources* 402, 147 (2018).
31. A.U. Rahman, I. Ahmad, and A.S. Malik, *J. Energy Storage* 29, 101365 (2020).
32. L. Hu, and Y. Cui, *Energy Environ. Sci.* 5, 6423 (2012).
33. K. Jost, G. Dion, and Y. Gogotsi, *J. Mater. Chem. A* 2, 10776 (2014).
34. M.F. El-Kady, and R.B. Kaner, *Nat. Commun.* 4, 1475 (2013).
35. Y. Shi, X. Wang, J. Luo, and Q. Xie, *J. Mater. Sci. Mater. Electron.* 30, 3692 (2019).
36. J. Yu, J. Wu, H. Wang, A. Zhou, C. Huang, H. Bai, L. Li, and A.C.S. Appl, *Mater. Interfaces* 8, 4724 (2016).
37. P. Shabeeba, K.K. Thasneema, M.S. Thayyil, M.P. Pillai, and C.V. Niveditha, *Mater. Res. Express* 4, 85501 (2017).
38. P. Bhargava, W. Liu, M. Pope, T. Tsui, and A. Yu, *Electrochim. Acta* 358, 136846 (2020).
39. K. Kopczyński, and G. Lota, *Electrochem. Commun.* 107, 106538 (2019).
40. R. Bernasconi, M. Zebarjadi, and L. Magagnin, *J. Electroanal. Chem.* 758, 163 (2015).
41. P. Sebastian, E. Valles, and E. Gómez, *Electrochim. Acta* 123, 285 (2014).
42. A.P. Abbott, K. El Ttaib, G. Frisch, K.J. McKenzie, and K.S. Ryder, *Phys. Chem. Chem. Phys.* 11, 4269 (2009).
43. Y. Xiao, G. Yu, J. Yuan, J. Wang, and Z. Chen, *Electrochim. Acta* 51, 4218 (2006).
44. H. Li, C.-Y. Guo, and C.-L. Xu, *Biosens. Bioelectron.* 63, 339 (2015).
45. A. Khan, A. Rashid, R. Younas, and R. Chong, *Int. Nano Lett.* 6, 21 (2016).
46. E.D. Cabanillas, J. Desimoni, G. Punte, and R.C. Mercader, *Mater. Sci. Eng. A* 276, 133 (2000).
47. A. Azam, A.S. Ahmed, M. Oves, M.S. Khan, S.S. Habib, and A. Memic, *Int. J. Nanomed.* 7, 6003 (2012).
48. R. Sankar, P. Manikandan, V. Malarvizhi, T. Fathima, K.S. Shivashangari, and V. Ravikumar, *Spectrochim. Acta Part A Mol. Biomol. Spectrosc.* 121, 746 (2014).
49. P.M. Kulal, D.P. Dubal, C.D. Lokhande, and V.J. Fulari, *J. Alloys Compd.* 509, 2567 (2011).
50. D.P. Dubal, D.S. Dhawale, R.R. Salunkhe, V.S. Jamdade, and C.D. Lokhande, *J. Alloys Compd.* 492, 26 (2010).
51. B. Vidyadharan, I.I. Misnon, J. Ismail, M.M. Yusoff, and R. Jose, *J. Alloys Compd.* 633, 22 (2015).
52. J. Li, W. Lu, Y. Yan, and T.-W. Chou, *J. Mater. Chem. A* 5, 11271 (2017).
53. Z. Huang, A. Chen, F. Mo, G. Liang, X. Li, Q. Yang, Y. Guo, Z. Chen, Q. Li, and B. Dong, *Adv. Energy Mater.* 10, 2001024 (2020).
54. Q. Yang, Z. Huang, X. Li, Z. Liu, H. Li, G. Liang, D. Wang, Q. Huang, S. Zhang, and S. Chen, *ACS Nano* 13, 8275 (2019).
55. V.D. Patake, S.S. Joshi, C.D. Lokhande, and O.-S. Joo, *Mater. Chem. Phys.* 114, 6 (2009).
56. A. Pendashteh, M.F. Mousavi, and M.S. Rahmanifar, *Electrochim. Acta* 88, 347 (2013).
57. S. Shivakumara, T.R. Penki, and N. Munichandraiah, *ECS Electrochem. Lett.* 2, A60 (2013).
58. K. Xie, J. Li, Y. Lai, W. Lu, Z. Zhang, Y. Liu, L. Zhou, and H. Huang, *Electrochem. Commun.* 13, 657 (2011).
59. B. Ameri, S.S.H. Davarani, R. Roshani, H.R. Moazami, and A. Tadjarodi, *J. Alloys Compd.* 695, 114 (2017).
60. D.P. Dubal, G.S. Gund, C.D. Lokhande, and R. Holze, *Mater. Res. Bull.* 48, 923 (2013).
61. S. Shivakumara, T.R. Penki, and N. Munichandraiah, *Mater. Lett.* 131, 100 (2014).